Malaysian Journal of Chemistry, 2020, Vol. 22(3), 32-40
(Special Issue: *International Conference in Organic Synthesis - ICOS 2019, Universiti Teknologi MARA*)

Characterization of Interleaved Zinc-Layered Hydroxide-Salicylic with Sustained Release Property: A New Promising Ultraviolet Absorber

Nurain Adam[1,2], Sheikh Ahmad Izaddin Sheikh Mohd. Ghazali[2*], Nur Nadia Dzulkifli[2] and Cik Rohaida Che Hak[3]

[1]Faculty of Applied Sciences, Universiti Teknologi MARA, 40450 Shah Alam, Selangor Darul Ehsan, Malaysia
[2]Faculty of Applied Sciences, Universiti Teknologi MARA Negeri Sembilan, Kampus Kuala Pilah, Pekan Parit Tinggi, 72000, Kuala Pilah, Negeri Sembilan, Malaysia
[3]Industrial Technology Division, Malaysian Nuclear Agency, Bangi, 43000, Kajang, Malaysia
*Corresponding author (e-mail: sheikhahmadizaddin@uitm.edu.my)

Salicylic acid (SA) is a type of organic ultraviolet absorber that can cause health issues when used at high concentrations. Zinc-layered hydroxide (ZLH) with the chemical formula of $M^{2+}(OH)_{2-x}(A^{m-})_{x/m}\cdot nH_2O$, where M^{2+} is a divalent cation and A^{m-} is a counter anion with a negative charge, was used to maximize the efficiency of SA and simultaneously reduce its side effects. Zinc-layered hydroxide-salicylic (ZSA) was synthesized using a simple direct method and then characterized. Fourier transform infrared-attenuated total reflection (FTIR-ATR) spectroscopy showed the presence of a new peak aside from the sharp peak at 560 cm^{-1}, corresponding to the presence of zinc oxide (ZnO). A new basal spacing formed in X-ray diffraction (XRD) study at 16.05 Å and a peak disappeared between 30° and 40°. Thermogravimetric analysis/differential thermogravimetric analysis (TGA/DTG) indicated that ZSA was stable to heat exposure. Meanwhile, field emission scanning electron microscopy (FESEM) showed that ZnO has a non-uniform granular shape, whereas ZSA has a non-uniform flaky shape, indicating that SA was imbedded between the ZLH interlayer regions. Brunauer-Emmett-Teller (BET) method showed that ZSA was a mesoporous material (Type IV) after the interleave process. The sustained release properties were evaluated using ultraviolet-visible (UV-Vis) spectrophotometry to study the sustained release of different simulated media solutions. In conclusion, SA can be intercalated between the interlayer galleries of ZLH and can have a slow-release property.

Key words: Layered salts; salicylic acid; ultraviolet absorber

Received: December 2019; Accepted: June 2020

Salicylic acid (SA), which is also known as 2-hydroxybenzoic acid (Fig. 1), is the weakest organic ultraviolet B (UV-B) filter that has been used as a sunblock agent. Organic UV filters absorb radiation from the sun and produce an excited state of molecules that gives higher energy content, and the excess energy is dissipated by the emission of higher wavelength or relaxation by photochemical process [1]. Two types of organic filters are filters in personal care products (PCPs) for hair and cutaneous membrane protection from sunlight, and filters for UV stabilizers used in various products, such as plastics and paints that protect polymers and pigments against photodegradation and prevent discoloring [2]. UV filter residues can be found in river water, lake water, seawater, and groundwater. The sediments and biota are toxic and could affect reproductive activity [3], as well as the normal development of aquatic and terrestrial organisms [4].

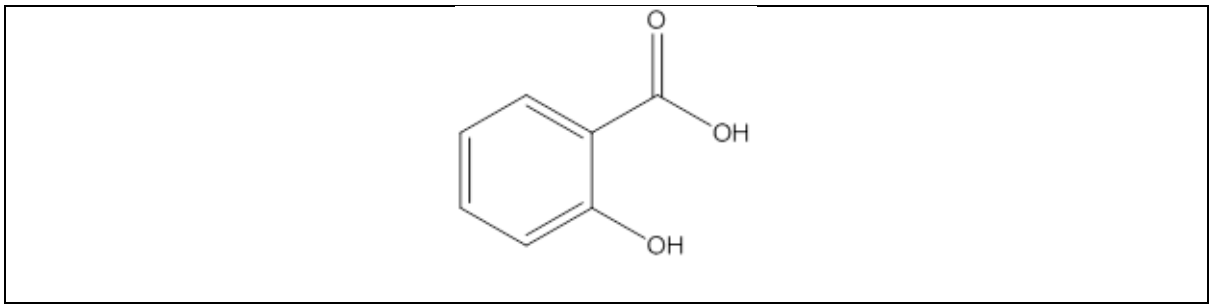

Figure 1. Chemical structure of salicylic acid

†Paper presented at the International Conference in Organic Synthesis (ICOS 2019), 9-10 December 2019, Universiti Teknologi MARA.

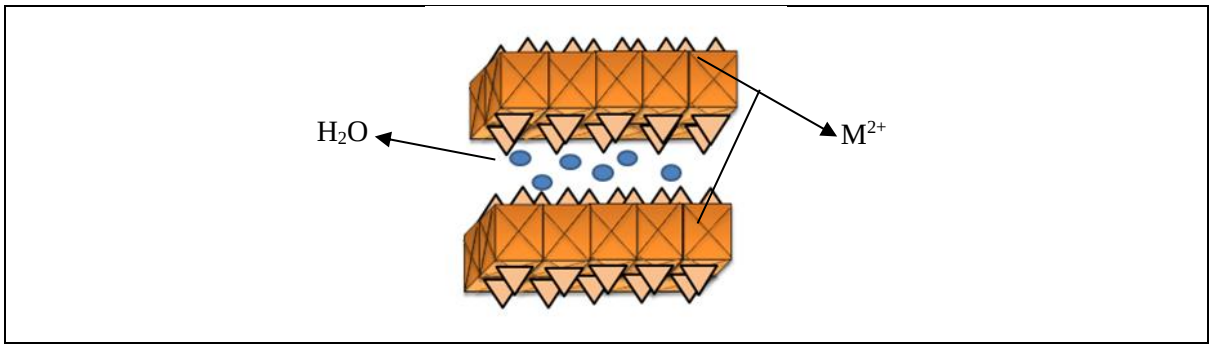

Figure 2. Illustration of ZLH structure

The incorporation of SA into layered materials can minimize adverse effects and increase the efficiency of scattering and absorbing UV radiation from the sun. Layered double hydroxides (LDHs) are the most common layered materials that have been extensively studied for their capability to exchange anions between their interlayer regions. Layered hydroxide salt (LHS) with certain divalent metallic cations is another type of layered material known to have a similar capability to LDH. The structure of LHS is known as an alternating sequence of modified brucite-like hydroxide and interlayer anions that are structurally similar to LDH [5]. A general formula that defines LHS is $M^{2+}(OH)_{2-x}(A^{n-})_{x/n}\cdot mH_2O$, where M^{2+} is a divalent metallic cation and A^{n-} is a counter anion. Zinc-layered hydroxide is a family of LHS that contains layers of octahedrally coordinated zinc. A quarter of them are displaced, leaving an empty octahedral site forming cationic centers and tetrahedrally coordinated at the top and bottom of the octahedral sheets [6], as illustrated in Fig. 2. The purpose of choosing ZLH instead of LDH as the layered compound is due to the lower interest in investigating ZLH as one of the layered compounds or materials.

The intercalation of SA into the interlayer region of ZLH can be performed using a simple direct method, in which zinc oxide (ZnO) is selected as a starting precursor. ZnO can act as an inorganic sunscreen agent that scatters and reflects ultraviolet A (UV-A) and B (UV-B) radiation, as well as prevents skin irritation and disruption of the endocrine system [7]. Zinc is known as a type of essential mineral for humans, which is used by certain enzymes for synthesizing and degrading lipids, proteins, nucleic acids, and carbohydrates [8]. Zinc is also used for its semiconducting properties, unique antibacterial and antifungal properties, wound healing, and high catalytic and photochemical activity [9]. Once the intercalation is completed, zinc-layered hydroxide-salicylic (ZSA) will go through physicochemical tests to determine the interaction between the inorganic-organic hybrid compounds. In this study, the release of ZSA in different salt solutions was studied by simulating various actual conditions, and the kinetic capabilities of the hybrid compound were evaluated.

MATERIALS AND METHODS

Salicylic acid (Sigma, > 99%), ZnO (R&M, 98%), sodium hydroxide (NaOH) (R&M, 99%), sodium carbonate (Na_2CO_3) (R&M, 99.5%), sodium phosphate (Na_3PO_4) (R&M, 99.2%), sodium chloride (NaCl) (Sigma, 99%), and deionized water were used throughout the experiment.

The inorganic-organic hybrid compound was synthesized using a simple direct method, where 0.2 g of pure ZnO was mixed with 0.8 M salicylate anion (salicylic acid solution) in 100 mL solution with an ethanol-to-water ratio of 2:1. The pH of the solution was adjusted to pH 7 ± 0.5 using 2 M NaOH. The mixture was mixed and stirred well for 3 h at room temperature. The obtained precipitate solution underwent an aging process in an oil bath shaker at 70°C for 18 h. The obtained slurry was centrifuged and washed thrice using distilled water. After that, the samples were stored for characterization.

Fourier transform infrared-attenuated total reflectance (FTIR-ATR) spectra were obtained using a FTIR spectrophotometer (Thermo-USA) to determine the functional groups of the hybrid compound. The powder X-ray diffraction (PXRD) pattern was obtained via Rigaku Mini-2 using Cu Kα radiation to study the basal spacing value. Field emission scanning electron microscopy (FESEM) images were obtained using Carl Zeiss SUPRA 40VP. Brunauer-Emmett-Teller (BET) method was used to investigate the specific surface areas of the nanocomposites, whereby around 1–2 g of the nanocomposites was weighed and tested with Micromeritics Gemini 2375. Thermogravimetric analysis was conducted with differential thermal analysis using NETZSCH TG 209. In this part, 10 mg of each sample was placed in an alumina crucible and heated at the temperature range from 37 to 800°C with a heating rate of 10°C min^{-1} [10].

The investigation of the release behavior of SA from the interlayered region was conducted using an ultraviolet-visible (UV-Vis) spectrophotometer at λ_{max} = 231 nm by placing 0.3 mg of ZSA nanocomposites in three types of 0.05 M salt solutions

(i.e., NaCl, Na_2CO_3, and Na_3PO_4) to simulate the conditions on skin, air, and soil. The simulation was done to understand the release of SA from the interlayer region of LDH based on the concentration effect of chloride ion (sweat on the skin), phosphate ion (soil), and air (the presence of carbon dioxide).

RESULTS AND DISCUSSION

The FTIR spectra for ZnO, SA, and 0.8 M ZSA are shown in Fig. 3. ZnO showed two significant peaks at 454 cm^{-1} and 560 cm^{-1} that indicated N-O vibration. SA contained OH stretching dimer with overlapping C-H vibration from 3300 cm^{-1} to 2600 cm^{-1}. The presence of C=O, C=C stretching, C-O, and C-H at 1654 cm^{-1}, 1482 cm^{-1}, 1293 cm^{-1}, and 757 cm^{-1}, respectively, indicated the significant peaks for SA. The FTIR peak for ZSA showed several peaks that typically exist in a pure SA compound, whereas the disappearance of the starting precursors indicated that SA intercalated between the ZLH interlayer structures. The presence of a broad peak at 3379 cm^{-1} indicated the presence of OH stretching dimer due to hydrogen bond formation [11]. ZSA also showed the presence of C=O group, symmetric stretching of C=C group, C-O group, and C-H group at 1623 cm^{-1}, 1467 cm^{-1}, 1249 cm^{-1}, and 755 cm^{-1}, respectively, suggesting that SA intercalated between the interlayer regions of ZLH. However, some of the peaks in ZSA shifted from their original or pure SA peaks due to the interaction of the organic anion with the ZLH interlayer structure [12, 13]. Meanwhile, the shift of wavenumber values was due to the possibility of host-guest interaction via hydrogen bonding between the COO^- of the organic anion with the OH group of the interlayer region, and guest-guest interaction through the conjugation of phenyl groups of interlayer ions related to various compositions and synthesis paths [14].

The PXRD patterns of intercalated compounds of 0.8 M ZSA and ZnO are presented in Fig. 4. Five important sharp peaks from 30° to 65° (2.8 Å, 2.6 Å, 2.4 Å, 1.9Å, 1.6Å, and 1.4Å) related to the reflections of 100, 002, 101, and 102 lattice planes [6] indicated that ZnO was a pure compound with high crystallinity [15]. Meanwhile, for 0.8 M ZSA, the pattern showed that the high-intensity peaks shifted to the lower regions of 2θ (i.e., 16.05 Å, 8.00 Å, and 5.37 Å), indicating that SA intercalated between the interlayer regions of ZLH with a well-formed and high crystallinity structure. The shifting of ZA into the lower area of 2θ was directly related to basal spacing, which was then followed by clear harmonic peaks, depending on the quality of the long-range order of the layered packing [16]. The even d-spacing values of reflection peaks for the intercalated compound with the ratio of 1, 2, and 3 indicated that the intercalated compound was in a good formation with the orderly stacked interlayer [12]. The increase in basal spacing was due to the bigger molecular size of SA anion compared to the size of water molecules present between the ZLH interlayer regions.

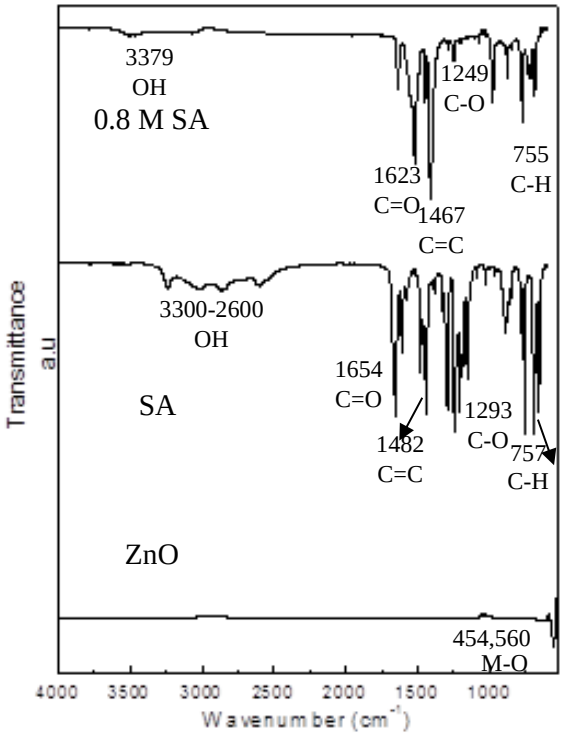

Figure 3. FTIR spectra for ZnO, 0.8 M SA, and ZSA

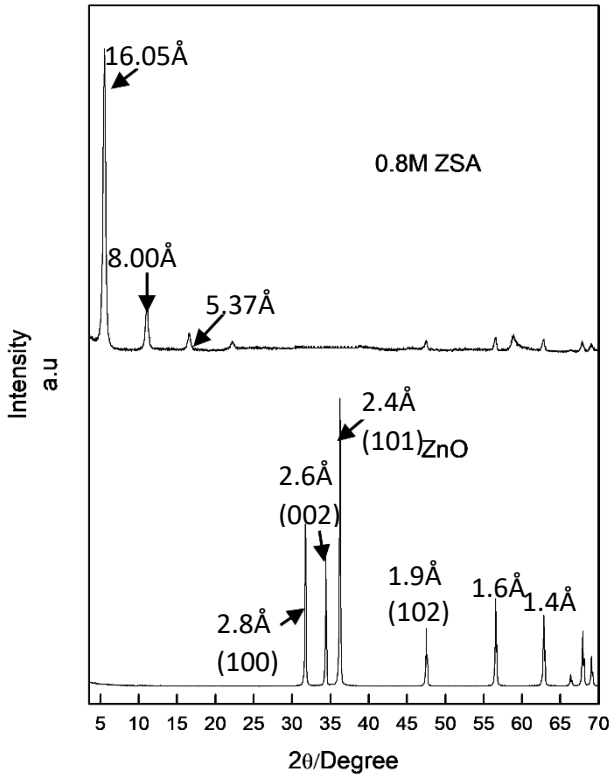

Figure 4. PXRD patterns for ZnO and 0.8 M ZSA

The mechanisms for the intercalation of the organic anion with ZnO followed the dissociation-deposition mechanisms, which occurred in three steps [17,18]. The first step was the formation of $Zn(OH)_2$ layers on the surface of ZnO when ZnO was introduced to water (hydrolysis). Then, the newly formed $Zn(OH)_2$ was more susceptible to acid compared to ZnO, which then formed Zn^{2+} and OH^-. Lastly, Zn^{2+}, OH^-, and the organic anion (i.e., salicylate anion (SA^-)) in the solution formed the layered compound and the process occurred continuously until all ZnO phases and $Zn(OH)_2$ phases were completely used to form the layered compound. The increase in the interlayer space could be calculated by considering the average basal spacing of ZSA (i.e., 16.05 Å). The calculated gallery height of 8.65 Å was obtained by subtracting the value of ZLH (i.e., 4.8 Å) and 2.6 Å for each zinc tetrahedron. SA was arranged in a bilayer, where the COO^- in the X-axis was positioned at the upper and bottom of the interlayer region of ZLH, as shown in Fig. 5. From the FESEM images, as depicted in Fig. 6, it could be concluded that ZnO had non-uniform granular surfaces. Meanwhile, the intercalated compound of 0.8 M SA with ZLH showed a combination of flaky and agglomerated shapes with a non-uniform structure.

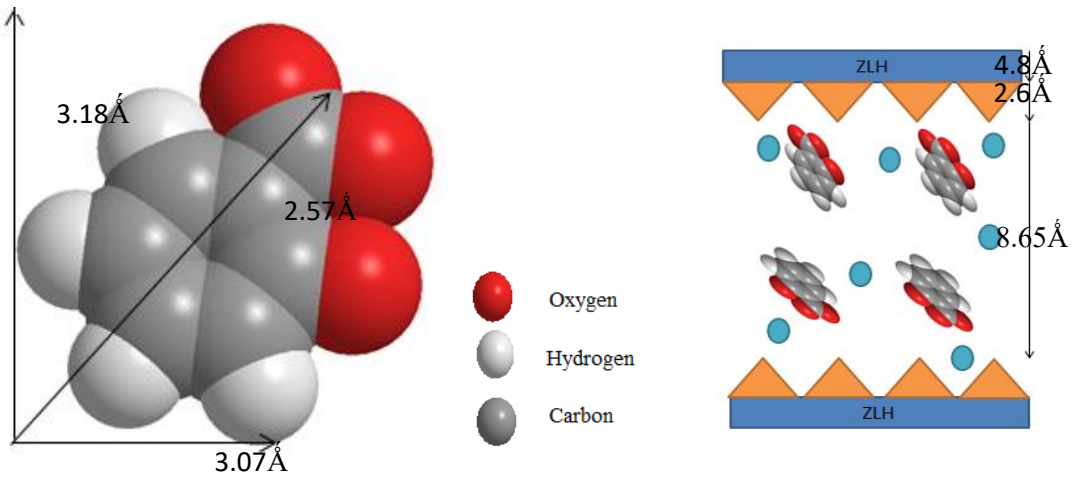

Figure 5. Spatial orientation of SA and the illustration of SA arrangement between the ZLH interlayer regions

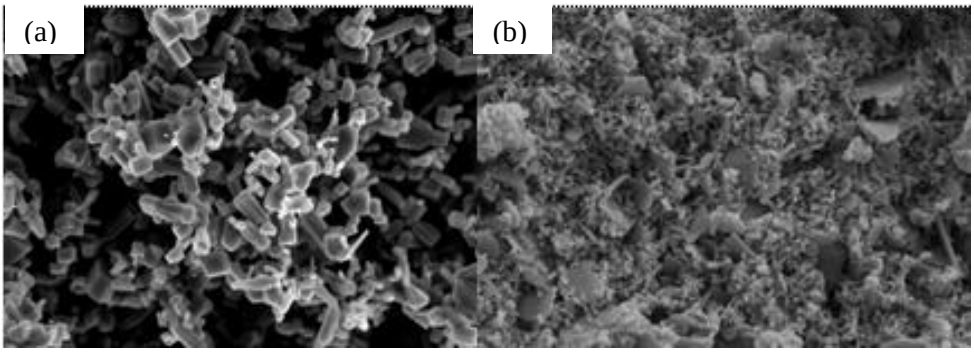

Figure 6. FESEM images of (a) ZnO and (b) 0.8M ZSA at 20,000× magnification

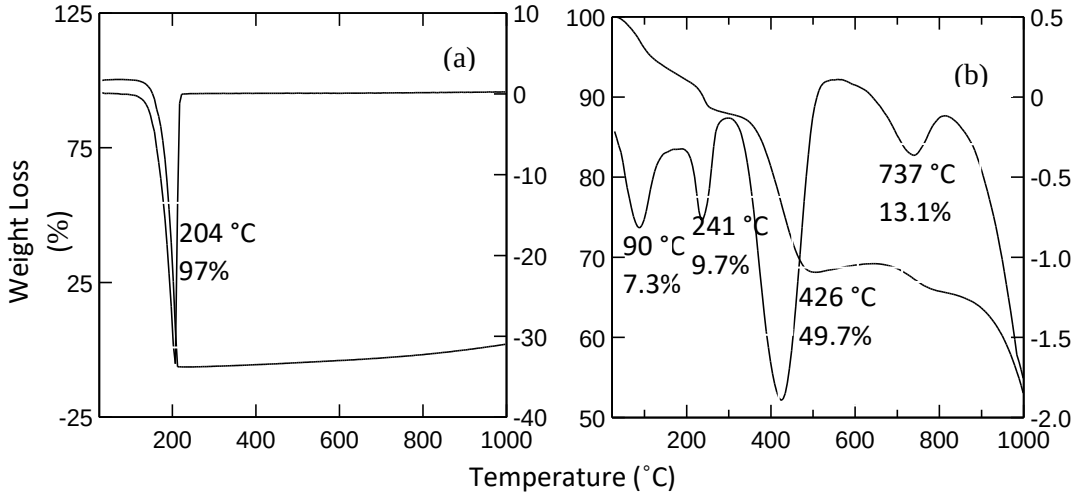

Figure 7. TGA/DTG thermograms for (a) SA and (b) 0.8 M ZSA

Thermogravimetric analysis/differential thermogravimetric analysis (TGA/DTG) measurements of SA and 0.8 M ZSA are shown in Fig. 7. SA showed only a single decomposition peak at 204°C with 97% decomposition. The decomposition of 0.8 M ZSA occurred between 50 and 800°C. The first and second decomposition at 90°C with 7.3% weight loss and 241°C with 9.7%, respectively, were attributed to the presence of water in the composite organic-inorganic ZSA. The decomposition was attributed to the loss of physisosorbed water molecules in the first decomposition and intercalated water structure [19]. The following decomposition occurred at 426°C was attributed to the decomposition of the organic anion with 49.7% loss. The decomposition of hydroxide layers occurred at 737°C with 13.1% decomposition. The TGA/DTG of ZSA and SA thermograms indicated that the intercalated compound was stable toward heat compared to SA in its pure state. The stability was identified from the organic-inorganic interaction of the negatively charged carboxylate group (COO^-) organic anion (SA) and positively charged Zn^{2+} inorganic interlayer region. The increase in thermal stability was due to the charge densities and the ability of the anion to be retained between the layers [16].

The nitrogen adsorption-desorption isotherms of ZnO and 0.8 M ZSA are shown in Fig. 8. The isotherms indicated that the precursor and ZSA were Type IV isotherms, and according to the International Union Pure and Applied Science Chemistry (IUPAC) classifications, both were mesoporous type materials. The adsorbate uptake for ZnO with relative pressure from 0.0 to 0.6 and the optimum absorbed nitrogen (N_2) of 4.11 cm^3/g indicated a low capacity for N_2 uptake [19]. Meanwhile, the intercalated compound of ZLH and 0.8 M SA underwent adsorption at 0.0–0.8 with 23.14 cm^3/g. The desorption branches for both ZnO and ZSA showed a type A hysteresis loop. However, a narrower loop was observed in ZnO compared to the ZSA intercalated compound, showing a different pore texture before and after the intercalation process. The increase in surface area from 4.11 m^2/g for ZnO to 23.14 m^2/g for the intercalated ZSA compound (Table 1) indicated that the larger surface area of the sorbent offered more active adsorption sites and better adsorption capacity [20]. Besides, 21.85% of C and 2.39% of H indicated the presence of organic anion with the calculated loading of 35.35%.

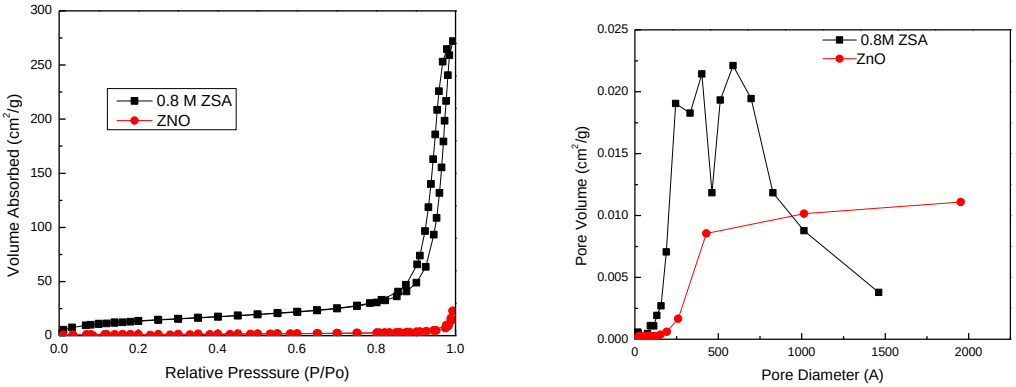

Figure 8. Adsorption-desorption isotherms and pore size distributions of ZnO and 0.8 M ZSA

Table 1. Physiochemical properties of ZnO and 0.8 M ZSA

	Surface Properties							Percent Loading (%)
	BET Surface Area (m^2/g)	BET Average Diameter (Å)	BJH Average Diameter (Å)	C%	H%	N%	S%	
ZnO	4.11	345.27	315.01	nd	nd	nd	nd	-
ZSA	23.14	298.78	324.72	21.85	2.39	0	0	35.35

The controlled release properties of ZSA using three different salt solutions are presented in Fig. 9. The fast release of SA was observed during the first 500 min for all salt solutions. The release behavior indicated that all solutions reached equilibrium starting from 10,000 min with the release percentages of 45%, 25%, and 20% of SA into phosphate, carbonate, and chloride salt solutions, respectively. The capability of SA to leach from the ZLH interlayer region was due to the exchange capability of the layered compound, which then formed a new hybrid compound. Anions with higher negative charge interact more strongly with the positively charged ZLH; thus, these anions easily and readily replace the existing anion in the ZLH interlayer region [21]. This phenomenon can be observed from the release properties shown in Fig. 9, whereby the release percentage of SA into PO_4^{3-} salt solution was much higher than CO_3^{2-} and Cl^- salt solutions. Thus, it could be concluded that the charges affect the release property of the anion from the ZLH interlayer region, in the order of PO_4^{3-} < CO_3^{2-} < Cl^-, with the slow percentage of SA release.

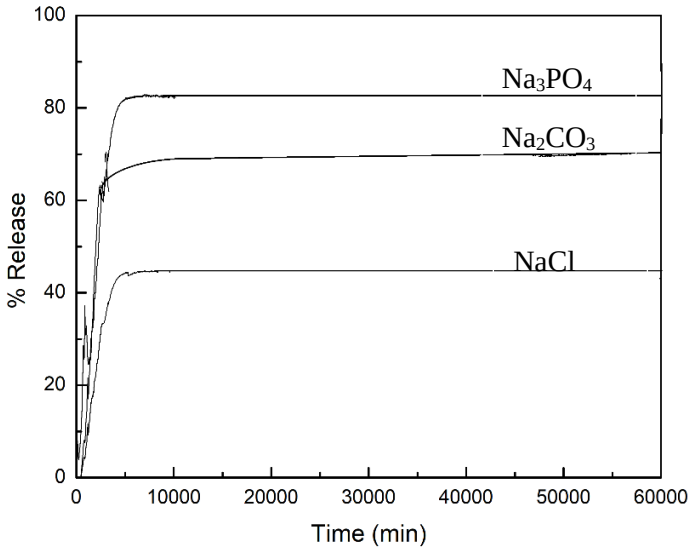

Figure 9. Controlled release of ZSA into NaCl, Na_2CO_3, and Na_3PO_4

The kinetic release of SA from the interlayer galleries of ZLH was analyzed using various kinetic models: zero-, first-, and second-order models. The linear correlation coefficient (R^2) values were obtained from the linear fitting, as shown in Table 1. The values of R^2 were calculated using zero-order (Eq. 1), first-order (Eq. 2), and pseudo-second-order (Eq. 3) models [22]:

$$Ct = kt + c \quad (1)$$

$$-\log(1-C) = kt + c \quad (2)$$

$$t/Ct = 1/k_2Ceq^2 + (1/qe)t \quad (3)$$

where Ceq is the concentration of anion at equilibrium, Ct is the concentration of anion at time *t*, C is the percentage release of anion, and c is a constant.

Table 2. Linear correlation coefficient, and rate constant and half-time for pseudo-second-order models

	Linear Correlation Coefficient (R^2)			Pseudo-Second-Order	
	Zero-Order	First-Order	Pseudo-Second-Order	Rate Constant, k	Half-Time
NaCl	0.0222	0.0225	0.9837	0.776×10^{-4}	29.95
Na_2CO_3	0.0168	0.0179	1.0000	0.097	1.7930
Na_3PO_4	0.0169	0.0195	0.9856	6.619×10^{-4}	162.08

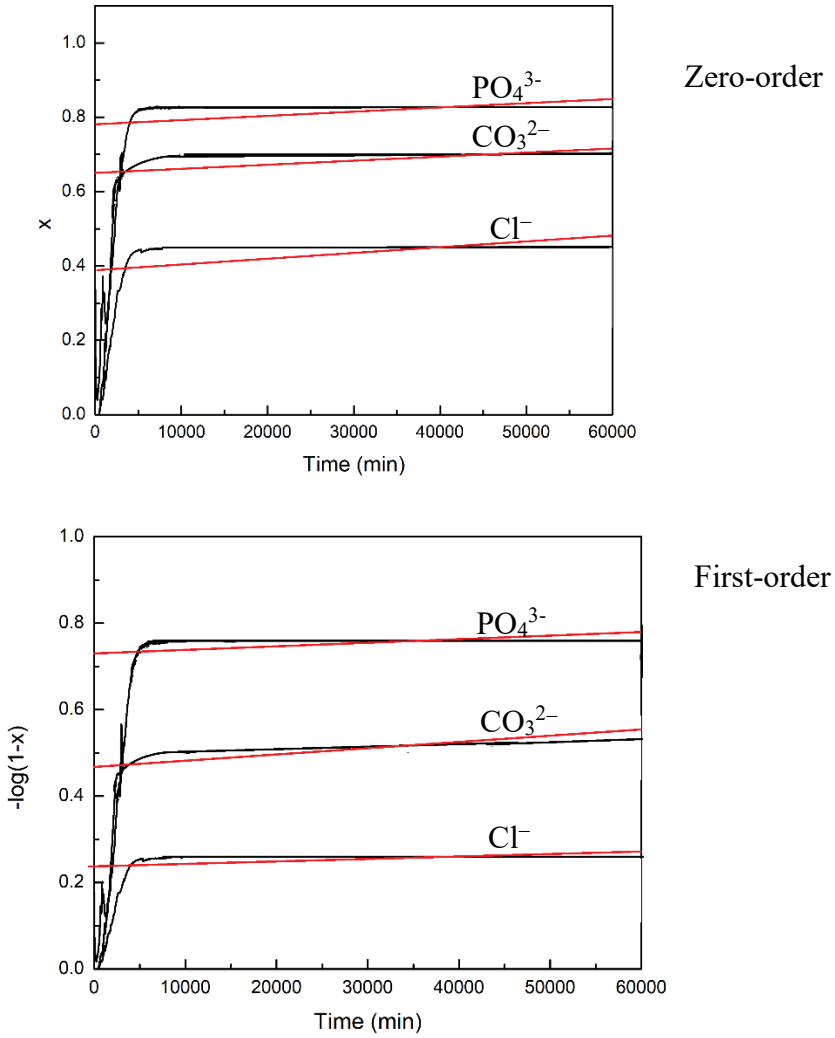

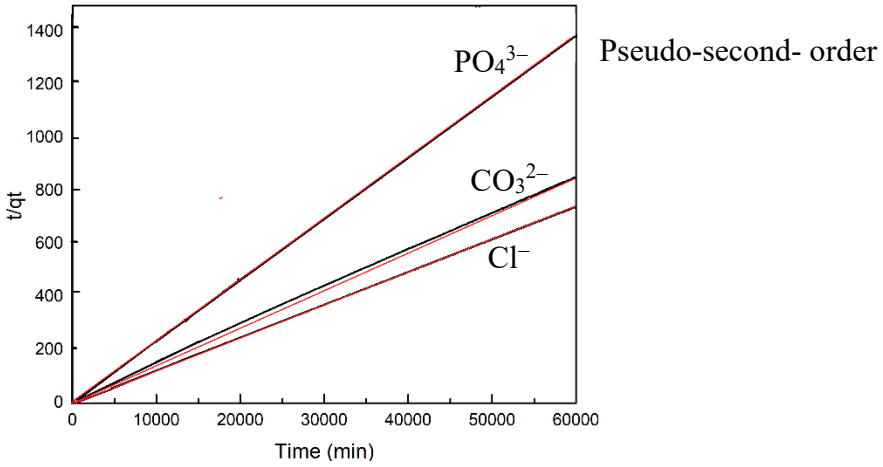

Figure 10. Release profiles of SA from the nanohybrid of the aqueous media using zero-order, first-order, and pseudo-second-order models

Based on the data tabulated in Table 2, the zero-order model gave the lowest R^2 and the model could not explain the release mechanism of SA. The release mechanism of SA from the ZLH interlayer region followed the pseudo-second-order kinetic model with the highest R^2 values compared to the other two kinetic models. The release mechanism is known to be divided into two phases, whereby the first stage is the rapid release 'burst effect' phase, followed by the second stage of the slow release phase [23]. The release of SA is known by the dissolution of SA from the interlayer region of ZLH through the solvent, which followed the release of salt anion solution in the order of $PO_4^{3-} < CO_3^{2-} < Cl^-$.

CONCLUSION

Based on the results, the FTIR-ATR spectra and PXRD patterns are correlated with each other, where C=O, C-O, C=C, and OH vibration modes were present with high intensity peaks at the lower region of 2θ with a value of 16.05 Å. TGA/DTG indicated that ZSA was stable toward heat exposure, and FESEM images showed that ZnO has a non-uniform granular shape. Meanwhile, the ZSA non-uniform flaky shape indicated that SA was embedded between the ZLH interlayer regions. BET showed that ZSA was a mesoporous compound. Finally, the release of SA depended on the charge density of the solution that followed the pseudo-second-order kinetic model.

ACKNOWLEDGEMENT

The authors would like to thank the Fundamental Research Grant Scheme (FRGS/1/2016/STG01/ UITM/02/4) for financial support. The authors would also like to extend the gratitude to Universiti Teknologi MARA (UiTM), UiTM Kuala Pilah branch, and the Malaysian Nuclear Agency for the facilities provided.

REFERENCES

1. Ramos, S., Homem, V., Alves, A., Santos, L. (2015) Advances in analytical methods and occurrence of organic UV-filters in the environment - A review. *Science of the Total Environment*, **526**, 278–311.

2. Langford, K. H., Reid, M. J., Fjeld, E., Øxnevad, S., Thomas, K. V. (2015) Environmental occurrence and risk of organic UV filters and stabilizers in multiple matrices in Norway. *Environment International*, **80**, 1–7.

3. Ramos, S., Homem, V., Alves, A., Santos, L. (2016) A review of organic UV-filters in wastewater treatment plants. *Environment International*, **86**, 24–44.

4. Molins-Delgado, D., Gago-Ferrero, P., Díaz-Cruz, M. S., Barceló, D. (2016) Single and joint ecotoxicity data estimation of organic UV filters and nanomaterials toward selected aquatic organisms. Urban groundwater risk assessment. *Environmental Research*, **145**, 126–134.

5. Newman, S. P., Jones, W. (1999) Comparative Study of Some Layered Hydroxide Salts Containing Exchangeable Interlayer Anions. *Journal of Solid State Chemistry*, **148(1)**, 26–40.

6. Ahmad, R., Hussein, M. Z., Wan Abdul Kadir, W. R., Sarijo, S. H., Yun Hin, T. Y. (2015) Evaluation of Controlled-Release Property and Phytotoxi-city Effect of Insect Pheromone Zinc-Layered Hydroxide Nanohybrid Intercalated with Hexenoic Acid. *Journal of Agricultural and Food Chemistry*, **63(51)**, 10893–10902.

7. Lu, P. J., Huang, S. C., Chen, Y. P., Chiueh, L. C., Shih, D. Y. C. (2015) Analysis of titanium dioxide and zinc oxide nanoparticles in

cosmetics. *Journal of Food and Drug Analysis*, **23(3)**, 587–594.

8. Barahuie, F., Hussein, M. Z., Abd Gani, S., Fakurazi, S., Zainal, Z. (2014) Anticancer nanodelivery system with controlled release property based on protocatechuate-zinc layered hydroxide nanohybrid. *International Journal of Nanomedicine*, **9(1)**, 3137–3149.

9. Elumalai, K., Velmurugan, S. (2015) Green synthesis, characterization and antimicrobial activities of zinc oxide nanoparticles from the leaf extract of Azadirachta indica (L.). *Applied Surface Science*, **345**, 329–336.

10. Wang, Y., Wu, P., Li, B., Zhu, N., Dang, Z. (2011) In-depth study on intercalating threonine into layered double hydroxides. *Applied Clay Science*, **53(4)**, 615–620.

11. Villegas, J. C., Giraldo, O. H., Laubernds, K., Suib, S. L. (2003) New layered double hydroxides cotaining intercalated manganese oxide species: Synthesis and characterization. *Inorg. Chem.*, **42(18)**, 5621–5631.

12. Ahmad, R., Hussein, M. Z., Sarijo, S. H., Rasidah, W., Abdul, W., Hin, T. Y. (2016) Synthesis and characteristics of vopaleric acid-zinc layered hydroxide intercalation material for insect pheromone-controlled release formulation. *Journal of Materials*, 2016: 1–9.

13. Bashi, A. M., Hussein, M. Z., Zainal, Z., Tichit, D. (2013) Synthesis and controlled release properties of 2,4-dichlorophenoxy acetate-zinc layered hydroxide nanohybrid. *Journal of Solid State Chemistry*, **203**, 19–24.

14. Bashi, A. M., Haddawi, S. M., Dawood, A. H. (2011) Synthesis and Characterizations of two Herbicides with Zn/Al Layered double hydroxide nano hybrides. *Journal of Kerbala University*, **9(1)**, 9–16.

15. Salleh, N. M., Mohsin, S. M. N., Sarijo, S. H., Ghazali, S. A. I. S. M. (2017) Synthesis and Physico-Chemical Properties of Zinc Layered Hydroxide-4-Chloro-2-Methylphenoxy Acetic Acid (ZMCPA) Nanocomposite. *IOP Conference Series: Materials Science and Engineering*, **204(1)**, 1–6.

16. Arizaga, G. G. C., Satyanarayana, K. G., Wypych, F. (2007) Layered hydroxide salts: Synthesis, properties and potential applications. *Solid State Ionics*, **178(15-18)**,1143–1162.

17. Jaafar, A. M., Anuar, A. N., Hashim, N., Ayob, F. H. (2016) Intercalation Study of Curcumin into Zinc Layered Hydroxide. *Malaysian Journal of Analytical Sciences*, **20(6)**, 1359–1364.

18. Hussein, M. Z. Bin, Ghotbi, M. Y., Yahaya, A. H., Abd Rahman, M. Z. (2009) The effect of polymers onto the size of zinc layered hydroxide salt and its calcined product. *Solid State Sciences*, **11(2)**, 368–375.

19. Al Ali, S. H. H., Al-Qubaisi, M., Hussein, M. Z., Zainal, Z., Hakim, M. N. (2011) Preparation of hippurate-zinc layered hydroxide nanohybrid and its synergistic effect with tamoxifen on HepG2 cell lines. *International Journal of Nanomedicine*, **6(1)**, 3099–3111.

20. Asiabi, H., Yamini, Y., Shamsayei, M. (2017) Highly selective and efficient removal of arsenic(V), chromium(VI) and selenium(VI) oxyanions by layered double hydroxide intercalated with zwitterionic glycine. *Journal of Hazardous Materials*, **339**, 239–247.

21. Cai, J., Zhao, X., Zhang, Y., Zhang, Q., Pan, B. (2018) Enhanced fluoride removal by La-doped Li/Al layered double hydroxides. *Journal of Colloid and Interface Science*, **509**, 353–359.

22. Ghazali, S. A. I. S. M., Hussein, M. Z., Sarijo, S. H. (2013) 3,4-Dichlorophenoxyacetate Inter-leaved into Anionic Clay for Controlled Release Formulation of a New Environmentally Friendly Agrochemical. *Nanoscale Research Letters*, **8(1)**, 1–8.

23. Djebbi, M. A., Elabed, A., Bouaziz, Z., Sadiki, M., Elabed, S., Namour, P., Amara, A. B. H. (2016) Delivery system for berberine chloride based on the nanocarrier ZnAl-layered double hydroxide: Physicochemical characterization, release behavior and evaluation of anti-bacterial potential. *International Journal of Pharmaceutics*, **515(1-2)**, 422–430.